NOVEL OPPORTUNITIES FOR SUB-meV INELASTIC X-RAY SCATTERING AT HIGH-REPETITION RATE SELF-SEEDED X-RAY FREE-ELECTRON LASERS

Oleg Chubar, Brookhaven National Laboratory, New York, USA
Gianluca Geloni, Anders Madsen, European XFEL GmbH, Hamburg, Germany
Vitali Kocharyan, Evgeni Saldin, Svitozar Serkez, DESY, Hamburg, Germany
Yuri Shvyd'ko, Advanced Photon Source, Argonne National Laboratory, Argonne, IL 60439, USA
John Sutter, Diamond Light Source Ltd, Didcot, Oxfordshire, OX11 0DE, UK

Abstract

Inelastic x-ray scattering (IXS) is an important tool for studies of equilibrium dynamics in condensed matter. A new spectrometer recently proposed for ultra-high-resolution IXS (UHRIX) has achieved 0.6 meV and 0.25 nm^{-1} spectral and momentum transfer resolutions, respectively [1]. However, further improvements down to 0.1 meV and 0.02 nm^{-1} are required to close the gap in energy-momentum space between high and low frequency probes. We show that this goal can be achieved by further improvements in x-ray optics and by increasing the spectral flux of the incident x-ray pulses. UHRIX performs best at energies from 5 to 10 keV, where a combination of self-seeding and undulator tapering at the SASE2 beamline of the European XFEL promises up to a hundred-fold increase in average spectral flux compared to nominal SASE pulses at saturation, or three orders of magnitude more than possible with storage-ring based radiation sources. Wave-optics propagation shows that about 7×10^{12} ph/s in a 90-μeV bandwidth can be achieved on the sample. This will provide unique new possibilities for IXS. Extended information about our work can be found in [2].

INTRODUCTION

Momentum resolved inelastic x-ray scattering (IXS) is a technique introduced [3, 4] and widely used [5–9] at synchrotron radiation facilities for studies of atomic-scale dynamics in condensed matter. A photon with energy E_i and momentum $\boldsymbol{K}_i$ changes its energy and momentum to E_f and $\boldsymbol{K}_f$ in a inelastic scattering process in the sample and leaves behind a collective excitation with energy $\varepsilon = E_i - E_f$ and momentum $\boldsymbol{Q} = \boldsymbol{K}_i - \boldsymbol{K}_f$, respectively. IXS provides access to dynamics on a length scale $\lambda = 2\pi/Q$ and a time scale $t = 2\pi\hbar/\varepsilon$ simultaneously. Presently, together with IXS there are a few inelastic scattering techniques allowing probes of a limited region in the time-length scale: in fact, a gap remains in experimental capabilities between the low-frequency (visible and ultraviolet light) and the high-frequency (x-rays and neutrons) inelastic scattering techniques. Because of this, dynamics in the range from about 1-100 picosecond (ps) on atomic- and meso-scales is still inaccessible. However, this region is of vital importance for disordered systems and, therefore, to the study of many outstanding problems in condensed matter dynamics, such as the nature of the liquid to glass transition.

IXS could in principle penetrate this unexplored dynamic range of excitations[1], but this would require solving two long-standing challenges. First, IXS spectrometers in their traditional implementation have not improved the best numbers in energy ($\simeq$ 1.5 meV) and momentum transfer ($\simeq$ 1.5 nm^{-1}) resolutions for the past 20 years [10, 11]. Second, the IXS signal is very weak. Hence, more efficient IXS spectrometers with better resolution and more powerful x-ray sources are required to advance the field. Recently, a new type of dispersive spectrometer was tested for the first time. This ultra-high-resolution IXS (UHRIX) spectrometer [1] achieved a spectral resolution of 0.6 meV at a momentum transfer down to 0.25 nm^{-1}. Additionally, the spectral contrast improved by an order of magnitude compared to the traditional IXS spectrometers [3, 10–14]. To sharpen the desired resolution to 0.1 meV and 0.02-nm^{-1} and to ensure higher countrates, we propose to further develop the angular dispersive x-ray optical scheme [15, 16] and to replace scanning IXS spectrometers with broadband imaging spectrographs [17][2].

Complementarily, high-repetition rate seeded x-ray free-electron lasers (XFELs) hold the promise to overcome the problem of weak IXS signals. Low-gain x-ray free-electron laser oscillators (XFELOs) may in time produce a spectral flux of up to $10^{14} - 10^{15}$ photons/s/meV [19, 20], but currently they are still under development [21]. High-gain XFELs under operation are limited, in average flux, by their low repetition rate [22, 23]. In contrast, at the European XFEL [24], owing to superconducting accelerator technology, Self-Amplified Spontaneous Emission (SASE) will allow for the production of average output fluxes of about 10^{12} photons/s/meV at 9 keV (the optimum working energy of the UHRIX setup), which is already more than one order of magnitude greater than at synchrotron radiation facilities [9]. The spectral flux can be further substantially increased by self-seeding [25, 26], which will be first be available, at the European XFEL, at the SASE2 beamline [27]. Another order of magnitude increase in flux can be gained by tapering the magnetic field of the seeded undulator [28–35].

[1] INS cannot enter this region because of the kinematic limitation. The low-frequency probes cannot enter this region because their photon wavelengths are too long.

[2] A Fourier-transform IXS technique has been demonstrated recently [18], which could be considered as a powerful complementary approach for studies of *non-equilibrium* excitation with ultra-high spectral resolution.

ISBN 978-3-95450-134-2

Pre-Release Snapshot 30-Sep-2015 00:00
Copyright © 2015 CC-BY-3.0 and by the respective authors

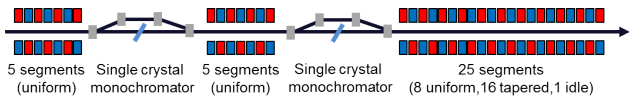

Figure 1: Layout of the baseline SASE2 undulator (35 segments).

In this work we propose to enable UHRIX in combination with an optimized configuration of the SASE2 x-ray source exploiting self-seeding and undulator tapering techniques in order to reach more than 10^{14} photons/s/meV, the same figure estimated in Ref. [36]. This may become a real game-changer for ultra-high-resolution x-ray spectroscopy, for IXS in particular, and for the studies of dynamics in disordered systems.

HIGH AVERAGE FLUX X-RAY SOURCE FOR ULTRA-HIGH-RESOLUTION IXS

The implementation of hard x-ray self-seeding (HXRSS) at European XFEL [27] will be based on a two cascade scheme in order to deal with the heat-load on the crystals at the high-repetition rate of the facility (up to 27000 X-ray pulses per second distributed in ten macropulses with up to 2700 pulses each). HXRSS will first be enabled at the SASE2 undulator line, which includes 35 segments, each consisting of 5 m long undulators, for a total of 175 m of magnetic length with an undulator period of 40 mm. We could then operate the SASE2 baseline in HXRSS mode followed by post-saturation tapering according to the scheme in Fig. 1, which optimizes the average output spectral flux around the optimum working point of the UHRIX setup, 9 keV. For seeding purposes we considered the (004) symmetric Bragg reflection from a 100 μm thick crystal. We performed numerical simulations of the high average-flux source in Fig. 1 using the code GENESIS [37]. Simulations are based on a statistical analysis consisting of 100 runs. Start-to-end simulations [38] yield the input information about the 250 pC, 17.5 GeV electron beam used for our study, which is fed into GENESIS.

The first five undulator segments work in the SASE mode, and yield the output power and spectrum in Fig. 2(a) and (b), respectively. The filtering process performed by the first crystal is illustrated in Fig. 2(c) and (d). The x-ray pulse then proceeds through the second undulator in Fig. 1, where it seeds the electron beam. Power and spectrum at the exit of the second undulator are shown in Fig. 2(e) and (f), respectively. This figure shows seed amplification in competition with the SASE process, given the relatively low seed power level from the first part of the setup. This is particularly evident in the time domain, where the reader can see the seeded pulse following about 20 μm after the SASE pulse. Note that the power levels in the two pulses are about the same. Moreover each of the pulses (seeded and SASE) carries about the same energy as the initial SASE pulse incident on the first crystal, for a total incident average energy per pulse of about

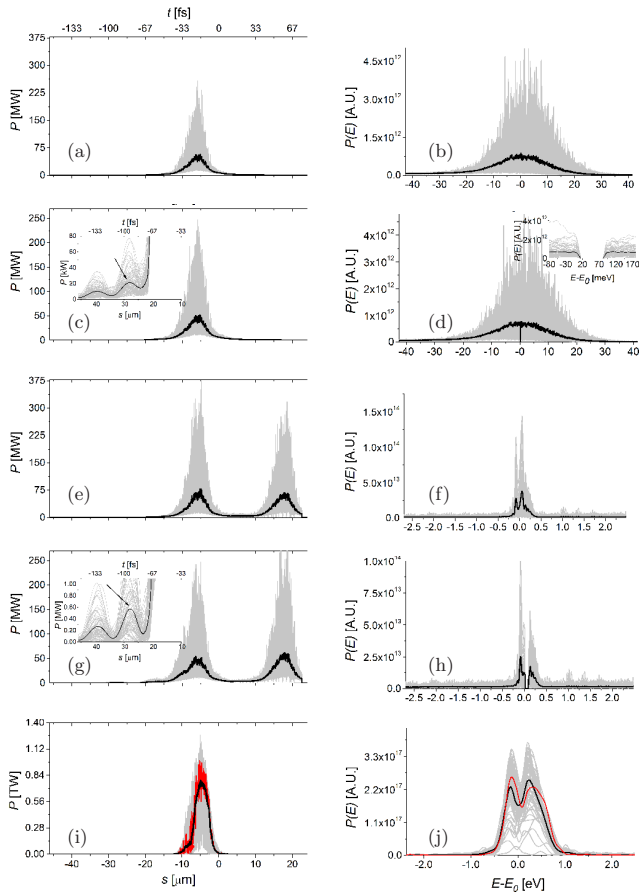

Figure 2: Power distribution and spectrum of the x-ray pulse along the undulator: (a) and (b) at the exit of the first undulator (5 segments); (c) and (d) after the first HXRSS monochromator; (e) and (f) at the exit of the second undulator (5 segments); (g) and (h) after the second HXRSS monochromator; (i) and (j) at the exit of the setup. Grey lines refer to single shot realizations, the black line refers to the average over a hundred realizations. The insets in (c) and (h) are an enlarged part of the main plot, showing the seed appearing after the filtering process. The black arrows indicate the position of the seed relative to the electron slice with maximum current. The red lines in graphs (i) and (j) refer to the particular FEL shot that is used for wavefront propagation simulations (see Section 'UHRIX OPTICS').

2.7 μJ, still within the heat-load limits. In the frequency domain, one notices a greatly increased peak power spectral density for the seeded signal [compare Fig. 2(d) and (f)] while the SASE pulse contributes a wide-bandwidth, noisy background. The fact that the power spectral density for the seed signal is larger than that for SASE by about an order of magnitude (roughly corresponding to the ratio of the SASE bandwidth to the seeded bandwidth) is what actually allows the x-ray beam to impinge on the second HXRSS crystal at relatively low power, but with a large signal (seeded) to noise (SASE) ratio, thus reducing heat loading effects by about one

Pre-Release Snapshot 30-Sep-2015 00:00

Copyright © 2015 CC-BY-3.0 and by the respective authors

ISBN 978-3-95450-134-2

order of magnitude compared to a single-chicane scheme. The filtering process performed by the second crystal is illustrated in Fig. 2(g) and (h), respectively. After this, the seed signal is amplified to saturation and beyond, exploiting a combination of HXRSS with post-saturation tapering.

Tapering is implemented by changing the K parameter of the undulator segment by segment. The tapering law used in this work [2] has been implemented on an empirical basis, in order to optimize the spectral density of the output signal. On the average, we expect to be able to produce pulses of about 11 mJ energy. The beam shape is nearly round with a FWHM size of about 50 μm, and a FWHM divergence of about 1.8 μrad. The final output of our setup is presented in Fig. 2(i) and (j), respectively, in terms of power and spectrum.

This result should be compared with the output power and spectrum for SASE at saturation, which corresponds to the *conventional* mode of operation foreseen for the European XFEL. Considering as before an average over 100 shots, the peak power for the SASE saturation case is about 4×10^{10} W, while for the seeded case in Fig. 2(i), it has increased to 7.5×10^{11} W. This corresponds to an increase in flux from about 7×10^{11} photons per pulse to about 7×10^{12} photons per pulse. This increase of about one order of magnitude is due to tapering. Moreover, the final SASE spectrum has a FWHM of about 11.6 eV, corresponding to a relative bandwidth of about 1.2×10^{-3} while, due to the enhancement of longitudinal coherence, the seeded spectrum has a FWHM of about 0.94 eV, corresponding to a relative bandwidth of about 1×10^{-4}.

Summing up, we obtain more than one order of magnitude increase in peak power due to tapering, and a bit less than an order of magnitude decrease in spectral width due to seeding. Combining the two effects, we obtain an increase of slightly over two orders of magnitude in spectral flux density from the SASE to the seeded-tapered case. This corresponds to about 2.1×10^{14} ph/s/meV for the seeded-tapered case, compared to about 1.5×10^{12} ph/s/meV in the case of SASE at saturation.

UHRIX OPTICS

Ultra-high-resolution IXS (UHRIX) studies with the 0.1-meV spectral and the 0.02-nm^{-1} momentum transfer resolution require a significant amount of x-ray photons with an energy $E_0 = 9.13185$ keV and a momentum $K = E_0/\hbar c = 46.27598$ nm^{-1} to be delivered onto the sample within a $\Delta E \lesssim 0.1$ meV spectral bandwidth, with a transverse momentum spread $\Delta K \lesssim 0.02$ nm^{-1}, and concentrated on the sample on a spot of $\Delta s \lesssim 5$ μm (FWHM) in diameter. The aforementioned fixed photon energy E_0 is required by the use of the (008) Bragg backreflection from a Si crystal, one of the central components of the ultra-high-resolution optics, presented in detail in [2].

We consider a scenario in which the UHRIX instrument is installed at a SASE2-undulator beamline of the European XFEL. In particular, we consider an option of integrating

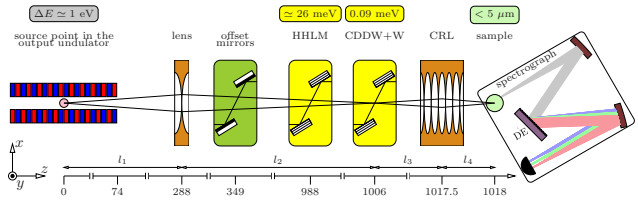

Figure 3: Main optical components of the proposed UHRIX instrument at the SASE2-undulator beamline of the European XFEL shown schematically together with the output undulator. Optical components are presented as pictographs at certain distances from the source position measured at the beam waist in the SASE2 undulator, which is at 74 m from undulator's downstream end. See text for descriptions.

UHRIX into the 'Materials Imaging and Dynamics' (MID) instrument [39], presently under construction at the European XFEL. A schematic view of optical components essential to deliver photons with the required properties on the sample for UHRIX studies is shown in Fig. 3. Optics are shown as pictographs at certain distances from the source. The source position is around 74 m inside the undulator. This number was determined by back-propagation in free space of the XFEL radiation from the undulator end.

The main optical components are as follows. A biconcave parabolic refractive lens [40], creates a secondary source on the 6-bounce angular dispersive ultra-high-resolution CDDW+W monochromator. This is essential in order to achieve a tight focal spot size on the sample because it eliminates the blurring that the strong angular dispersion of the CDDW+W monochromator would otherwise cause [17]. The CDDW+W monochromator then selects a 0.1 meV spectral bandwidth from the incident x-ray beam. CDDW+W is a modification of a CDW-type angular dispersive monochromator [16, 41, 42], which uses a three-step process of collimation (C), angular dispersion (D), and wavelength selection (W) [43]. Finally, a parabolic compound refractive lens CRL [40, 44] focuses the monochromatic x-rays on the sample.

The x-ray spectrograph captures photons scattered from the source in a sufficiently large solid angle and images them in a spectral window a few meV wide with an 0.1-meV spectral resolution in the dispersion plane. The dispersing element (DE), a hard x-ray analog of optical diffraction gratings, is a key component of the spectrograph. The spectrograph is also capable of simultaneously imaging scattered intensity perpendicular to the dispersion plane in a range of 0.2-nm^{-1} with 0.01-nm^{-1} resolution.

Supplementary optical components include a pair of offset mirrors, which separate XFEL radiation from unwanted high-energy bremsstrahlung, and the two-bounce, two-crystal non-dispersive high-heat-load monochromator (HHLM). The HHLM narrows the 1-eV bandwidth of the incident x-rays to about 26 meV and thus reduces the heat-load onto the ultra-high-resolution CDDW+W monochromator by a fac-

ISBN 978-3-95450-134-2

Pre-Release Snapshot 30-Sep-2015 00:00

Copyright © 2015 CC-BY-3.0 and by the respective authors

tor of 36. The choice of optical elements of the UHRIX instrument and their design parameters were determined by dynamical theory calculations for monochromatization, and by geometrical optics for focusing.

Verification of the design parameters, determination of the efficiency of the system and calculation of the radiation characteristics were performed by wavefront propagation simulations from the XFEL source to the sample. GENESIS [37] calculates the original wavefront of the SASE radiation at the exit of the output undulator. SRW [45], calculates the wavefront after propagation from the undulator through each drift space and optical component in the beamline by using Fourier optics. Simulations of the diffracting crystals with SRW have just recently been made possible by the addition of a new module [46], which has already been applied to the design of the planned IXS beamline 10-ID at NSLS-II [47].

Results of the wavefront propagation simulations related to the sample area are presented graphically in Fig. 4. The spectral, time, spatial, and angular radiation pulse distributions and their parameters at the sample location (image plane at z = 1018 m in Fig. 3), are provided in captions to Fig. 4. The calculated radiation parameters at the sample location are in good agreement with design values obtained by the ray-transfer matrix approach and dynamical theory calculations. Thus, the wavefront propagation simulations confirm the soundness of the optical design of the UHRIX instrument worked out initially by the ray-transfer matrix approach and dynamical theory calculations. They also confirm the feasibility of the target specification.

The wavefront propagation simulations show that the spectral flux from the XFEL undulator can be transported to the sample through the UHRIX x-ray optics with a 30% efficiency and reach a remarkably high value of $\simeq 7 \times 10^{13}$ ph/s/meV. This number exceeds by more than three orders of magnitude the spectral flux numbers reported for the state of the art IXS instruments at synchrotron radiation facilities [9]. The specially designed crystal and focusing optics ensure that $\simeq 6.3 \times 10^{12}$ ph/s/meV photons on the sample can be concentrated in a spectral band of 0.09 meV, on the spot with a 3.3(V) $\times$ 6.5(H) μm^2 size, and with a momentum transfer spread of $\lesssim 0.015$ nm^{-1}.

DISCUSSION AND CONCLUSIONS

This article explores novel opportunities for ultra-high-resolution IXS (UHRIX) at high repetition rate XFELs unlocked by the recent demonstration of a conceptually new spectrometer [1] with unprecedented specifications (0.6 meV spectral resolution and 0.25 nm^{-1} momentum transfer), operating around 9 keV. Its exploitation, together with the broadband ultra-high-resolution imaging spectrograph proposed in [17] will make it possible to fill the energy-momentum gap between high and low frequency inelastic probes and to provide exciting new opportunities for studies of dynamics in condensed matter. In particular, UHRIX experiments can be enabled at the European XFEL, where an increase of more than three orders of magnitude in average spectral flux is expected compared to what is available today at synchrotrons. The gain is due to two main factors: firstly, the high repetition rate of the European XFEL, owing to the superconducting linac accelerator driver, which allows up to 27000 X-ray pulses per second, and secondly, the presence of long undulators, allowing the combined implementation of hard X-ray self-seeding (HXRSS) and post-saturation tapering techniques. In particular, a double-chicane HXRSS scheme increases the signal-to-noise ratio and eases the heat-load on the HXRSS crystals to a tolerable level. This scheme is expected to yield up to TW-level X-ray pulses. Simulations of pulse propagation up to the sample position through the UHRIX optics show that an unprecedented average spectral flux of 7×10^{13} ph/s/meV is feasible. The power delivered to the sample can be as high as 350 W/mm^2 and radiation damage can become a limitation but liquid jets and scanning setups for solid samples can be employed to circumvent eventual problems, see Ref. [39] and references therein.

ACKNOWLEDGMENTS

We are grateful to Massimo Altarelli for many useful discussions and support, and to Thomas Tschentscher, Serguei Molodtsov, Harald Sinn, Stephen Collins, Giulio Monaco, Alexei Sokolov, Kwang-Je Kim, Kawal Sawhney, Alexey Suvorov and Igor Zagorodnov for useful discussions and interest in this work. Work at the APS was supported by the U.S. Department of Energy, Office of Science, Office of Basic Energy Sciences, under Contract No. DE-AC02-06CH11357. The development of SRW code is supported in part by the US DOE Office of Science, Office of Basic Energy Sciences under SBIR awards DE-SC0006284 and DE-SC0011237.

REFERENCES

[1] Y. Shvyd'ko, S. Stoupin, D. Shu, S. P. Collins, K. Mundboth, J. Sutter, and M. Tolkiehn, Nature Communications **5:4219** (2014).

[2] O. Chubar et al., 'Novel opportunities for sub-meV inelastic X-ray scattering at high-repetition rate self-seeded X-ray free-electron lasers', http://arxiv.org/abs/1508.02632, DESY 15-140, (2015).

[3] E. Burkel, B. Dorner, and J. Peisl, Europhys. Lett. **3**, 957 (1987).

[4] E. Burkel, *Inelastic Scattering of X rays with Very High Energy Resolution*, vol. 125 of *Springer Tracts in Modern Physics* (Springer, Berlin, 1991).

[5] F. Sette, M. H. Krisch, C. Masciovecchio, G. Ruocco, and G. Monaco, Science **280**, 1550 (1998).

[6] E. Burkel, Rep. Prog. Phys. **63**, 171 (2000).

[7] M. Krisch and F. Sette, *Light Scattering in Solids IX* (Springer, Berlin, 2007), vol. 108 of *Topics in Applied Physics*, chap. Inelastic X-Ray Scattering from Phonons, pp. 317–370.

[8] G. Monaco, *Synchrotron Radiation* (Springer Berlin Heidelberg, 2015), chap. The High-Frequency Atomic Dynamics of Disordered Systems Studied by High-Resolution Inelastic X-Ray Scattering, pp. 461–482.

Pre-Release Snapshot 30-Sep-2015 00:00

Copyright © 2015 CC-BY-3.0 and by the respective authors

ISBN 978-3-95450-134-2

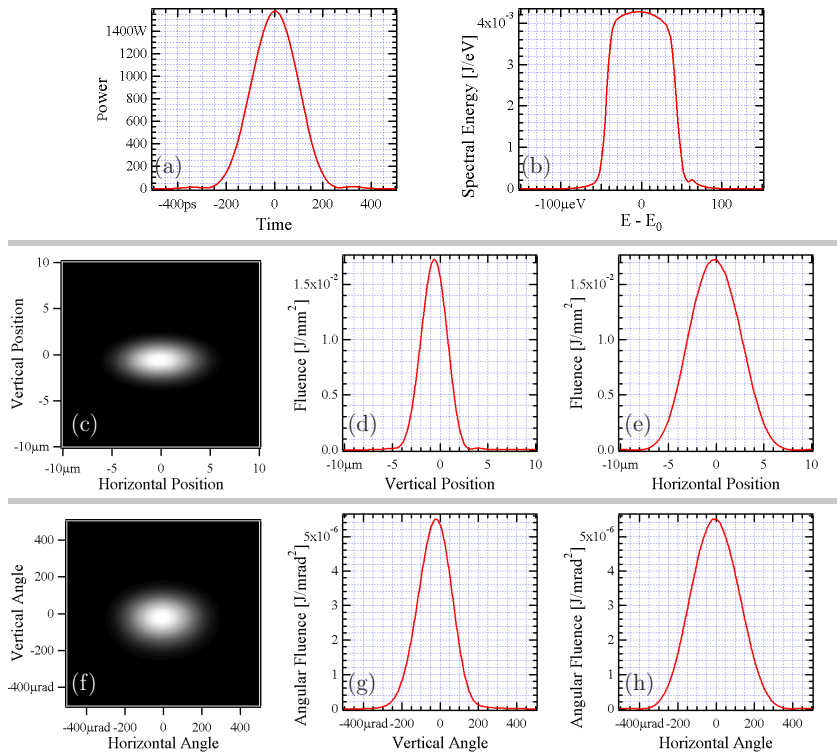

Figure 4: Time, spectral, spatial and angular distributions of the radiation pulse on the sample (z = 1018 m in Fig. 3). (a) Pulse power, pulse duration is ≃ 225 ps (FWHM) (b) Spectrum, spectral bandwidth is ≃ 0.090 meV (FWHM). (c) Spatial distribution, 2D plot; (d) vertical x-cut through the center of the fluence distribution; and (e) horizontal y-cut. Beam footprint size on the sample is 3.3 μm (V)×6.5 μm (H) (FWHM). (f) Angular distribution, 2D plot; (h) vertical cut through the center of the fluence distribution; and (g) horizontal cut. Beam divergence on the sample is 220 μrad (V)×310 μrad (H) (FWHM), corresponding to a 0.01 $\text{nm}^{-1} \times 0.015\ \text{nm}^{-1}$ transverse momentum spread.

[9] A. Q. R. Baron, arXiv:1504.01098 (2015).

[10] C. Masciovecchio, U. Bergmann, M. Krisch, G. Ruocco, F. Sette, and R. Verbeni, Nucl. Instrum. Methods Phys. Res. B **117**, 339 (1996).

[11] A. H. Said, H. Sinn, and R. Divan, Journal of Synchrotron Radiation **18**, 492 (2011).

[12] F. Sette, G. Ruocco, M. Krisch, U. Bergmann, C. Masciovecchio, Mazzacurati, G. Signorelli, and R. Verbeni, Phys. Rev. Lett. **75**, 850 (1995).

[13] A. Q. R. Baron, Y. Tanaka, D. Miwa, D. Ishikawa, T. Mochizuki, K. Takeshita, S. Goto, T. Matsushita, H. Kimura, F. Yamamoto, et al., Nucl. Instrum. Methods Phys. Res. A **467-468**, 627 (2001).

[14] H. Sinn, E. Alp, A. Alatas, J. Barraza, G. Bortel, E. Burkel, D. Shu, W. Sturhahn, J. Sutter, T. Toellner, et al., Nucl. Instrum. Methods Phys. Res. A **467-468**, 1545 (2001).

[15] Y. Shvyd'ko, S. Stoupin, K. Mundboth, and J. Kim, Phys. Rev. A **87**, 043835 (2013).

[16] S. Stoupin, Y. V. Shvyd'ko, D. Shu, V. D. Blank, S. A. Terentyev, S. N. Polyakov, M. S. Kuznetsov, I. Lemesh, K. Mundboth, S. P. Collins, et al., Opt. Express **21**, 30932 (2013).

[17] Y. Shvyd'ko, Phys. Rev. A **91**, 053817 (2015).

[18] M. Trigo, M. Fuchs, J. Chen, M. P. Jiang, M. Cammarata, S. Fahy, D. M. Fritz, K. Gaffney, S. Ghimire, A. Higginbotham, et al., Nature Physics **9**, 790–794 (2013).

[19] K.-J. Kim, Y. Shvyd'ko, and S. Reiche, Phys. Rev. Lett. **100**, 244802 (2008).

[20] R. R. Lindberg, K.-J. Kim, Y. Shvyd'ko, and W. M. Fawley, Phys. Rev. ST Accel. Beams **14**, 010701 (2011).

[21] T. J. Maxwell, J. Arthur, Y. Ding, W. M. Fawley, J. Frisch, J. Hastings, Z. Huang, J. Krzywinski, G. Marcus, K.-J. Kim, et al., in *Proceedings of the 2015 International Particle Accelerator Conference* (SLAC Publication: SLAC-PUB-16286, 2015).

[22] P. Emma, R. Akre, J. Arthur, R. Bionta, C. Bostedt, J. Bozek, A. Brachmann, P. Bucksbaum, R. Coffee, F.-J. Decker, et al., Nature Photonics **4**, 641 (2010).

[23] T. Ishikawa, H. Aoyagi, T. Asaka, Y. Asano, N. Azumi, T. Bizen, H. Ego, K. Fukami, T. Fukui, Y. Furukawa, et al., Nature Photonics **6**, 540–544 (2012).

[24] M. Altarelli, R. Brinkmann, M. Chergui, W. Decking, B. Dobson, S. Dusterer, G. Grübel, W. Graeff, H. Graafsma, J. Hajdu, et al., *XFEL: The European X-Ray Free-Electron Laser : Technical design report* (DESY, Hamburg, 2006).

[25] G. Geloni, V. Kocharyan, and E. Saldin, Journal of Modern Optics **58**, 1391 (2011a).

ISBN 978-3-95450-134-2

Pre-Release Snapshot 30-Sep-2015 00:00

Copyright © 2015 CC-BY-3.0 and by the respective authors

[26] J. Amann, W. Berg, V. Blank, F.-J. Decker, Y. Ding, P. Emma, Y. Feng, J. Frisch, D. Fritz, J. Hastings, et al., Nature Photonics **6** (2012).

[27] *XFELSEED, 'Design and construction of Hard X-ray Self-Seeding Setups for the European XFEL'*, Project approved in the framework of the coordinated German-Russian call for proposals 'Ioffe-Röntgen Institute' (2014).

[28] P. Sprangle, C.-M. Tang, and W. M. Manheimer, Phys. Rev. Lett. **43**, 1932 (1979).

[29] N. Kroll, P. Morton, and M. Rosenbluth, IEEE J. Quantum Electronics **QE-17**, 1436 (1981).

[30] T. J. Orzechowski, B. R. Anderson, J. C. Clark, W. M. Fawley, A. C. Paul, D. Prosnitz, E. T. Scharlemann, S. M. Yarema, D. B. Hopkins, A. M. Sessler, et al., Phys. Rev. Lett. **57**, 2172 (1986).

[31] W. M. Fawley, Z. Huang, K.-J. Kim, and N. A. Vinokurov, Nucl. Instrum. Methods Phys. Res. A **483**, 537 (2002).

[32] X. J. Wang, H. P. Freund, D. Harder, W. H. Miner, J. B. Murphy, H. Qian, Y. Shen, and X. Yang, Phys. Rev. Lett. **103**, 154801 (2009).

[33] G. Geloni, V. Kocharyan, and E. Saldin, arXiv:1007.2743 (2010), DESY 10-108.

[34] W. Fawley, J. Frisch, Z. Huang, Y. Jiao, H.-D. Nuhn, C. Pellegrini, S. Reiche, and J. Wu, Tech. Rep., SLAC National Accelerator Laboratory, Menlo Park, CA 94025, USA (2011), SLAC-PUB-14616.

[35] Y. Jiao, J. Wu, Y. Cai, A. W. Chao, W. M. Fawley, J. Frisch, Z. Huang, H.-D. Nuhn, C. Pellegrini, and S. Reiche, Phys. Rev. ST Accel. Beams **15**, 050704 (2012).

[36] X. Yang and Y. Shvyd'ko, Phys. Rev. ST Accel. Beams **16**, 120701 (2013).

[37] S. Reiche, Nucl. Instrum. Methods Phys. Res. A **429**, 243 (1999).

[38] I. Zagorodnov (2012), http://www.desy.de/fel-beam/s2e/.

[39] A. Madsen, J. Hallmann, T. Roth, and G. Ansaldi, Technical Design Report, XFEL.EU TR-2013-005, European X-Ray Free-Electron Laser Facility GmbH, Hamburg, Germany (2013).

[40] B. Lengeler, C. Schroer, J. Tümmler, B. Benner, M. Richwin, A. Snigirev, I. Snigireva, and M. Drakopoulos, J. Synchrotron Radiation **6**, 1153 (1999).

[41] Y. V. Shvyd'ko, M. Lerche, U. Kuetgens, H. D. Rüter, A. Alatas, and J. Zhao, Phys. Rev. Lett. **97**, 235502 (2006).

[42] Y. Shvyd'ko, S. Stoupin, D. Shu, and R. Khachatryan, Phys. Rev. A **84**, 053823 (2011).

[43] Y. Shvyd'ko, *X-Ray Optics – High-Energy-Resolution Applications*, vol. 98 of *Optical Sciences* (Springer, Berlin Heidelberg New York, 2004).

[44] A. Snigirev, V. Kohn, I. Snigireva, and B. Lengeler, Nature **384**, 49 (1996).

[45] O. Chubar and P. Elleaume, EPAC-98 Proceedings pp. 1177–1179 (1998).

[46] J. P. Sutter, O. Chubar, and A. Suvorov, Proc. SPIE **9209**, 92090L (2014).

[47] A. Suvorov, Y. Q. Cai, J. P. Sutter, and O. Chubar, Proc. SPIE **9209**, 92090H (2014).

Pre-Release Snapshot 30-Sep-2015 00:00

Copyright © 2015 CC-BY-3.0 and by the respective authors

ISBN 978-3-95450-134-2